Identifying a Z' behind $b \to s\ell\ell$ anomalies at the LHC

M. Kohda and T. Modak

Department of Physics, National Taiwan University, Taipei 10617, Taiwan

A. Soffer

Tel Aviv University, Tel Aviv 69978, Israel

Recent $b \to s\ell\ell$ anomalies may imply the existence of a new Z' boson with left-handed $Z'bs$ and $Z'\mu\mu$ couplings. Such a Z' may be directly observed at LHC via $b\bar{s} \to Z' \to \mu^+\mu^-$, and its relevance to $b \to s\ell\ell$ may be studied by searching for the process $gs \to Z'b \to \mu^+\mu^-b$. In this paper, we analyze the capability of the 14 TeV LHC to observe the Z' in the $\mu^+\mu^-$ and $\mu^+\mu^-b$ modes based on an effective model with major phenomenological constraints imposed. We find that both modes can be discovered with 3000 fb^{-1} data if the $Z'bs$ coupling saturates the latest $B_s - \bar{B}_s$ mixing limit from UTfit at around 2σ. Besides, a tiny right-handed $Z'bs$ coupling, if it exists, opens up the possibility of a relatively large left-handed counterpart, due to cancellation in the $B_s - \bar{B}_s$ mixing amplitude. In this case, we show that even a data sample of $\mathcal{O}(100)$ fb^{-1} would enable discovery of both modes. We further study the impact of a $Z'bb$ coupling as large as the $Z'bs$ coupling. This scenario enables discovery of the Z' in both modes with milder effects on the $B_s - \bar{B}_s$ mixing, but obscures the relevance of the Z' to $b \to s\ell\ell$. Discrimination between the $Z'bs$ and $Z'bb$ couplings may come from the production cross section for the $Z'b\bar{b}$ final state. However, we do not find the prospect for this to be promising.

I. INTRODUCTION

Bottom-quark transitions of $b \to s$ have been of great interest as a means for studying physics beyond the standard model (SM) since the observation of the decay $B \to K^*\gamma$ by the CLEO collaboration [1]. Involving a flavor-changing neutral current (FCNC), such processes are possible in the SM only at loop level, providing unique sensitivity to new physics (NP).

The high production rate and detection efficiency for bottom hadrons at the LHCb experiment have enabled precision tests that probe physics at high energy scales. Based on the Run-1 data, LHCb measurements of several observables related to $b \to s\ell^+\ell^-$ ($\ell = e$ or μ) transitions are in tension with SM predictions. The most notable discrepancies are found in the P'_5 [2] angular-distribution observable for the $B^0 \to K^{*0}\mu^+\mu^-$ decay [3,4], and in the lepton-flavor universality observables $R_K \equiv \mathcal{B}(B^+ \to K^+\mu^+\mu^-)/\mathcal{B}(B^+ \to K^+e^+e^-)$ [5] and $R_{K^*} \equiv \mathcal{B}(B^0 \to K^{*0}\mu^+\mu^-)/\mathcal{B}(B^0 \to K^{*0}e^+e^-)$ [6]. Moreover, measured differential branching ratios for exclusive $b \to s\mu^+\mu^-$ decays such as $B^0 \to K^0\mu^+\mu^-$, $B^+ \to K^+\mu^+\mu^-$, $B^+ \to K^{*+}\mu^+\mu^-$ [7], $B^0 \to K^{*0}\mu^+\mu^-$ [8], $B_s^0 \to \phi\mu^+\mu^-$ [9] and $\Lambda_b^0 \to \Lambda\mu^+\mu^-$ [10] are consistently lower than SM predictions in the dimuon-invariant mass range below the J/ψ threshold. ATLAS and CMS are also capable of studying $b \to s\mu^+\mu^-$ transitions. They have performed angular analyses for $B^0 \to K^{*0}\mu^+\mu^-$ with 8 TeV data [11,12], where the measured P'_5 by ATLAS supports the discrepancy found by LHCb while the measurements by CMS are in agreement with SM predictions. Belle [13] reports an angular analysis for $B \to K^*\ell^+\ell^-$, finding mild tension in P'_5 in the muon mode, but not in the electron mode. The measurements will be significantly improved with more data collected by LHC, as well as with the upcoming Belle II experiment [14].

While the statistical significance of each discrepancy is not large enough, there is excitement about the possibility that their combination might suggest the presence of NP. To investigate this possibility, global-fit analyses based on the effective Hamiltonian formalism have been performed by several groups (see Refs. [15–22] for studies that include the recent R_{K^*} [6] result). These fits find that the tensions in the $b \to s\ell\ell$ observables can be simultaneously alleviated to a great extent by a NP contribution in a single Wilson coefficient. Most authors find this to be the

coupling between the left-handed (LH) $b \to s$ current and either the LH or vector muon current.[1]

In particular, the findings of the global-fit analyses motivate studying a new gauge boson, Z', with FCNC interactions. Many phenomenological studies of such a Z' have been performed (see, e.g., [24–78]).

Produced at LHC via $b\bar{s} \to Z'$ and undergoing the decay $Z' \to \mu^+\mu^-$, the Z' may be discovered in dimuon resonance searches. Such a discovery by itself, however, would not reveal the relevance of the observed resonance to the $b \to s\ell\ell$ anomalies. Comparison with searches in the electron mode can test lepton-flavor universality in the Z' couplings, but one should also establish the coupling to the $b \to s$ current. In principle, this can be done with the decay $Z' \to b\bar{s}$. However, this decay is suppressed relative to $Z' \to \mu^+\mu^-$ due to the $B_s - \bar{B}_s$ mixing constraint, as we discuss below, and its detection suffers from overwhelming QCD background. On the other hand, the $Z'bs$ coupling can induce the process $gs \to Z'b$. Therefore, this coupling can be explored through production modes of the Z' at LHC.

In this paper, we investigate the prospects for direct observation of the Z', as well as determination of the flavor structure of its couplings at LHC, with $\sqrt{s} = 14$ TeV. We argue that achieving this dual goal requires measuring the cross sections of both $pp \to Z' + X$ and $pp \to Z'b + X$, where X refers to additional activity in the pp collision. We employ an effective-model description of the Z' couplings, and assume that it is the source of all the NP required to alleviate the tensions in $b \to s\mu^+\mu^-$. We focus mainly on the role of the $Z'bs$ coupling in the Z' production processes $pp \to Z' + X$ and $pp \to Z'b + X$. The constraints on the leptonic coupling of the Z' are much weaker than those on the $Z'bs$ coupling. Therefore, we use $Z' \to \mu^+\mu^-$ as the main discovery mode. As the LH $Z'bs$ coupling is accompanied by a LH $Z'bb$ coupling in many UV complete models (see, e.g., Refs. [31,51,58,61]), we also study scenarios in which the $Z'bb$ coupling is of the same order as the $Z'bs$ coupling. We note that a larger $Z'bb$ coupling implies larger cross sections and easier discovery of the Z' at the LHC, but obscures the role of the Z' in $b \to s\ell\ell$. Therefore, this case is not the focus of our work. We also consider the process $pp \to Z'b\bar{b} + X$ for discrimination between the $Z'bs$ and $Z'bb$ couplings, where the latter coupling uniquely contributes via $gg \to Z'b\bar{b}$.

We emphasize that our purpose is different from that of existing studies, which focus on discovery and/or constraint of the Z' rather than testing its role in $b \to s\ell\ell$. Recent studies on the impact of existing dimuon resonance searches on a Z' motivated by the $b \to s\ell\ell$ anomalies can be found, e.g., in Refs. [64,71]. Reference [71] also

studies the future sensitivity at the LHC, exploiting the use of additional b jets for background suppression. However, it targets a $Z'bb$ coupling that is much larger than the $Z'bs$ coupling. The future sensitivities at the LHC and a 100 TeV pp collider are studied in Ref. [72] with an extrapolation of existing ATLAS limit.

We show that the cross sections for $b\bar{s} \to Z'$ and $gs \to Z'b$ are limited by a rather tight constraint on the $Z'bs$ coupling, which originates from the $B_s - \bar{B}_s$ mixing. This severely restricts the discovery potential of the Z', unless the $Z'bb$ coupling is comparable or larger than the $Z'bs$ coupling. As the $B_s - \bar{B}_s$ mixing constraint is indirect, the actual limit on the $Z'bs$ coupling depends on the details of the UV-complete model. In particular, a nonzero right-handed (RH) $Z'bs$ coupling can drastically change the constraint, due to the large $(V - A) \otimes (V + A)$ term [79] in the $B_s - \bar{B}_s$ mixing amplitude. Although there is no strong indication of a RH $b \to s$ current in the majority of the global-fit analyses, even a tiny RH $Z'bs$ coupling would allow for a large LH $Z'bs$ coupling due to the cancellation. This would significantly boost the Z' production cross sections. We investigate the discovery potential in this case as well.

This paper is organized as follows. In Sec. II, we introduce the effective model for our collider study. In Sec. III, we evaluate existing phenomenological constraints on the relevant couplings of the Z' boson to quarks and leptons. This is carried out for two representative Z' mass values, $m_{Z'} = 200$ and 500 GeV. In Sec. IV, we study the signal and background cross sections for the three processes of interest, $pp \to Z' + X$, $Z'b + X$ and $Z'b\bar{b} + X$, given the coupling constraints. We then proceed to estimate the signal significances for the full integrated luminosity of the High-Luminosity LHC (HL-LHC) program, $\mathcal{L} = 3000$ fb^{-1}. In Sec. V, we discuss the impact of a tiny but nonzero RH $Z'bs$ coupling, which allows discovery with smaller integrated luminosities. Summary and discussions are given in Sec. VI.

II. EFFECTIVE MODEL

We describe the Z' couplings to the SM fermions with the effective Lagrangian

$$\mathcal{L} \supset -Z'_\alpha [g^L_{bb}\bar{b}\gamma^\alpha P_L b + g^L_{bs}(\bar{b}\gamma^\alpha P_L s + \bar{s}\gamma^\alpha P_L b)$$
$$+ g^L_{\mu\mu}(\bar{\mu}\gamma^\alpha P_L \mu + \bar{\nu}_\mu\gamma^\alpha P_L \nu_\mu) + g^R_{\mu\mu}\bar{\mu}\gamma^\alpha P_R \mu], \quad (1)$$

where $P_{L,R} = (1 \mp \gamma_5)/2$, and g^L_{bb}, g^L_{bs} and $g^{L,R}_{\mu\mu}$ are coupling constants. For simplicity, since no significant CP violation has been observed in the relevant observables, we take the couplings to be real. In addition to the LH $Z'bs$ coupling and LH and RH $Z'\mu\mu$ couplings motivated by the $b \to s\ell^+\ell^-$ global fits, we introduce the LH $Z'bb$ coupling predicted in many UV-complete models. We take $g^L_{\mu\mu}$ to also be the coupling to the muon neutrino, as required by

---

[1]However, we note the existence of a fit to other $B \to K^*\mu^+\mu^-$ observables [23], which indicates a NP contribution in the right-handed $b \to s$ current.

the $SU(2)_L$ gauge symmetry, and since observables containing neutrinos give meaningful constraints on the Z' parameters, as shown below. The RH $Z'bs$ coupling is not included at this stage, as it is discussed only in Sec. V.

Since we take $m_{Z'} \gg m_b$, we integrate out the Z' to obtain its contributions to the effective Hamiltonian for $b \to s\mu^+\mu^-$ transitions, given by

$$\Delta \mathcal{H}_{\text{eff}} = \mathcal{N}[C_9^{\text{NP}}(\bar{s}\gamma^\alpha P_L b)(\bar{\mu}\gamma_\alpha \mu)$$
$$+ C_{10}^{\text{NP}}(\bar{s}\gamma^\alpha P_L b)(\bar{\mu}\gamma_\alpha \gamma_5 \mu)] + \text{H.c.}, \quad (2)$$

where $\mathcal{N} = -\frac{\alpha G_F}{\sqrt{2}\pi} V_{tb} V_{ts}^*$, and

$$C_9^{\text{NP}} = \frac{g_{bs}^L g_{\mu\mu}^V}{\mathcal{N} m_{Z'}^2}, \qquad C_{10}^{\text{NP}} = \frac{g_{bs}^L g_{\mu\mu}^A}{\mathcal{N} m_{Z'}^2}, \quad (3)$$

are the Wilson coefficients, with the vector and axial-vector muon couplings defined by

$$g_{\mu\mu}^V \equiv \frac{g_{\mu\mu}^R + g_{\mu\mu}^L}{2}, \qquad g_{\mu\mu}^A \equiv \frac{g_{\mu\mu}^R - g_{\mu\mu}^L}{2}. \quad (4)$$

With the parametrization of the Cabibbo-Kobayashi-Maskawa (CKM) matrix in Ref. [80], $C_{9,10}^{\text{NP}}$ are treated as real to a good approximation.

Motivated by the global-fit analyses, we consider two possibilities for the chiral structure of the muon couplings: a vector coupling and a LH coupling. For each of these, we extract constraints on the couplings from global-fit analyses presented in Ref. [15]. The first analysis uses all available $b \to s\ell\ell$ data from LHCb, ATLAS, CMS and Belle. This yields the following two scenarios:

(i) Vector coupling ($g_{\mu\mu}^L = g_{\mu\mu}^R$) and, hence, $C_{10}^{\text{NP}} = 0$. In this case, the best-fit value is $\text{Re}C_9^{\text{NP}} = -1.11$, with a 2-standard-deviation (2σ) range of

$$-1.45 \leq \text{Re}C_9^{\text{NP}} \leq -0.75. \quad (5)$$

(ii) LH coupling ($g_{\mu\mu}^R = 0$), so that $C_9^{\text{NP}} = -C_{10}^{\text{NP}}$. For this scenario, the best-fit value is $\text{Re}C_9^{\text{NP}} = -\text{Re}C_{10}^{\text{NP}} = -0.62$, with a 2σ range of

$$-0.88 \leq \text{Re}C_9^{\text{NP}} = -\text{Re}C_{10}^{\text{NP}} \leq -0.37. \quad (6)$$

The authors of Ref. [15] also present results when taking into account only lepton-flavor universality observables, such as $R_{K^{(*)}}$ measured by LHCb [5,6] and the differences Q_4 and Q_5 [81] between angular observables in $B \to K^*\mu^+\mu^-$ and $B \to K^*e^+e^-$, measured by Belle [13]. This leads to the following two scenarios:

(i') In the case of vector coupling, the best-fit value is $\text{Re}C_9^{\text{NP}} = -1.76$, with $-3.04 \leq \text{Re}C_9^{\text{NP}} \leq -0.76$ at 2σ interval.

(ii') For the LH-coupling case, the best-fit value is found to be $\text{Re}C_9^{\text{NP}} = -\text{Re}C_{10}^{\text{NP}} = -0.66$, while at 2σ range $-1.04 \leq \text{Re}C_9^{\text{NP}} = -\text{Re}C_{10}^{\text{NP}} \leq -0.32$.

In the rest of the paper we explore scenario (i) in detail, and occasionally comment on differences with respect to the other scenarios. Generally, these differences are small and do not significantly affect our main results in Sec. IV.

III. ALLOWED PARAMETER SPACE

In Fig. 1 we show the various constraints on g_{bs}^L vs $g_{\mu\mu}^V$ in scenario (i), for the representative Z'-mass values of
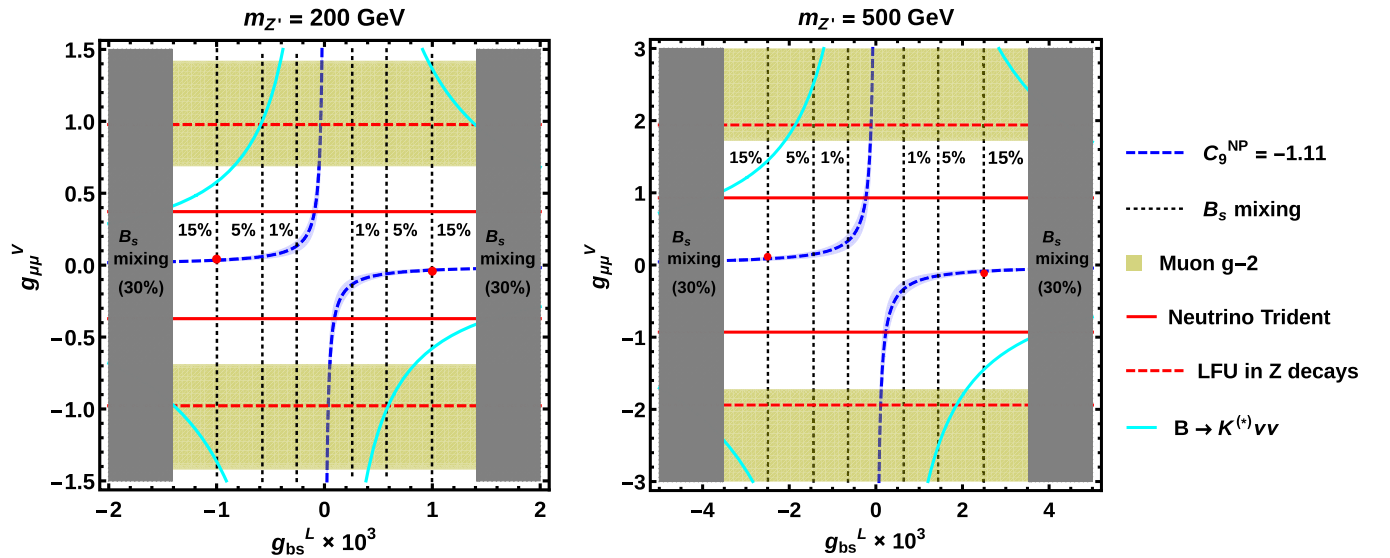
FIG. 1. Constraints on the vector $Z'\mu\mu$ coupling $g_{\mu\mu}^V = g_{\mu\mu}^L = g_{\mu\mu}^R$ vs the LH $Z'bs$ coupling g_{bs}^L (in units of 10^{-3}) in scenario (i), for $m_{Z'} = 200$ GeV (left) and 500 GeV (right). The red dots show the benchmark points discussed in Sec. IV. See the main text for details.

$m_{Z'} = 200$ and 500 GeV. The relevant inputs and constraint calculation methods are described in the remainder of this section.

Before embarking on this detailed description, we note that, as seen in Fig. 1, the limits on $g_{\mu\mu}^V$ are much weaker than those on g_{bs}^L. Therefore, the Z' is likely to decay primarily to leptons, so that its decays into quarks can be ignored. The leptonic-decay dominance simplifies the discussion. In fact, it is also essential for direct observation of the Z' at the LHC, since searches with $Z' \to b\bar{b}$, $b\bar{s}$ suffer from overwhelming QCD background. Thus, in the scenario (i), where $g_{\mu\mu}^L = g_{\mu\mu}^R \neq 0$, the dominant branching ratios are

$$\mathcal{B}(Z' \to \mu^+\mu^-) \simeq \frac{2}{3}, \qquad \mathcal{B}(Z' \to \nu_\mu\bar{\nu}_\mu) \simeq \frac{1}{3}. \quad (7)$$

In scenario (ii), each of these branching ratios is 50%.

To incorporate the results of $b \to s\ell\ell$ global fits, we use Eq. (3) to convert the 2σ constraints of Eq. (5) to the space of g_{bs}^L vs $g_{\mu\mu}^V$. The result is given by the blue hyperbolas in Fig. 1.

As an example of the impact of the choice of scenario among those listed in Sec. II, we note that in scenario (i'), the resulting values of $g_{\mu\mu}^V$ are generically higher than those shown in Fig. 1, and have a wider range. Although this somewhat changes the $Z' \to \mu^+\mu^-$ branching ratio, Eq. (7) is still satisfied. Therefore, the results we obtain in Sec. IV are not affected.

The most important constraint on the $Z'bs$ coupling comes from the B_s mixing. With the tree-level Z' exchange contribution, the total $B_s - \bar{B}_s$ mixing amplitude relative to the SM one (see, e.g., Ref. [82]) is given by

$$\frac{M_{12}}{M_{12}^{\mathrm{SM}}} = 1 + \frac{(g_{bs}^L)^2}{m_{Z'}^2} \left(\frac{g_2^2}{16\pi^2 v^2} (V_{tb}V_{ts}^*)^2 S_0 \right)^{-1}, \quad (8)$$

where $S_0 \simeq 2.3$ is an Inami-Lim function, g_2 is the $SU(2)_L$ gauge coupling, $v \simeq 246$ GeV, and a common QCD correction factor is assumed for the SM and NP contributions. The mass difference $\Delta m_{B_s^0} = 2|M_{12}|$ is precisely measured, at the per mill level [80], while the calculation of M_{12} suffers from various sources of uncertainty. One of the dominant uncertainties is the CKM factor, with an uncertainty of $\sim5\%$ [83,84]. The other is the hadronic matrix element, obtained from the lattice. The average of $N_f = 2 + 1$ lattice results compiled by FLAG in 2016 [85] implied a $\sim12\%$ uncertainty in M_{12}^{SM}. Recently, the situation was greatly improved with the advent of the accurate estimate by the Fermilab Lattice and MILC collaborations [86], which pushes down the uncertainty of the FLAG average to $\sim6\%$. (See the December 2017 update on the FLAG web site [85].) A global analysis of the CKM parameters by CKMfitter [83], published before the recent

lattice result [86], gives a constraint on M_{12} with NP as $|M_{12}/M_{12}^{\mathrm{SM}}| = 1.05_{-0.13}^{+0.14}$. On the other hand, the summer 2016 result [84] by UTfit, which includes the result of Ref. [86], constrains NP with a better precision: $|M_{12}/M_{12}^{\mathrm{SM}}| = 1.070 \pm 0.088$. As we assume g_{bs}^L to be real, the Z' contribution always enhances $|M_{12}|$. If one takes these uncertainties to be Gaussian, these results imply $|M_{12}/M_{12}^{\mathrm{SM}}| < 1.32$ [83] or 1.25 [84] at 2σ for the CKMfitter and UTfit results, respectively. In this paper, we explore NP contributions to $|M_{12}/M_{12}^{\mathrm{SM}}|$ at the level of up to 30%. Excluding larger contributions leads to the gray-shaded regions in Fig. 1. Future improvements in lattice calculations and measurements of the CKM parameters would tighten the constraint [87]. In Fig. 1, we illustrate the impact of possible future improvements by the vertical dotted lines for deviation of M_{12} from SM by 15% or 5%.

We note that while the CKMfitter [83] and UTfit [84] results are tolerant to a NP contribution that enhances $|M_{12}|$, there are studies that find the SM prediction of $\Delta m_{B_s^0} = 2|M_{12}|$ to be larger than the measured value, slightly favoring NP that reduces $|M_{12}|$. In particular, a recent study [77], which adopts the 2017 FLAG result [85], finds the SM prediction to be 1.8σ above the measured value. Their result can be read as $|M_{12}/M_{12}^{\mathrm{SM}}| \simeq 0.89 \pm 0.06$, which allows an enhancement by NP only up to $\sim1\%$ at 2σ. The rather small uncertainty is in part due to a smaller uncertainty of 2.1% assigned to the CKM factor. Addressing the discrepancy among the theoretical calculations is beyond the scope of this paper. Instead, the 1% vertical dotted lines are also shown in Fig. 1 for illustrating the impact of the result by Ref. [77].

The nonzero LH $Z'\mu\mu$ coupling implies also the existence of a $Z'\nu\nu$ coupling, due to $SU(2)_L$. Therefore, constraints are also set by $B \to K^{(*)}\nu\bar{\nu}$. The effective Hamiltonian for $b \to s\nu\bar{\nu}$ is [88]

$$\mathcal{H}_{\mathrm{eff}}^\nu = \mathcal{N} \sum_{\ell=e,\mu,\tau} C_L^\ell (\bar{s}\gamma^\alpha P_L b)[\bar{\nu}_\ell \gamma_\alpha (1 - \gamma_5)\nu_\ell] + \mathrm{H.c.}, \quad (9)$$

where $C_L^\mu = C_L^{\mathrm{SM}} + C_L^{\mathrm{NP}}$ and $C_L^\ell = C_L^{\mathrm{SM}}$ ($\ell = e$, τ) are lepton-flavor dependent Wilson coefficients. The SM contribution is lepton-flavor universal and is given by $C_L^{\mathrm{SM}} = -X_t/s_W^2$ with $X_t = 1.469 \pm 0.017$ [89]. The Z' contribution is given by

$$C_L^{\mathrm{NP}} = \frac{g_{bs}^L g_{\mu\mu}^L}{2\mathcal{N} m_{Z'}^2}. \quad (10)$$

Normalizing $B \to K^{(*)}\nu\bar{\nu}$ branching ratios by the SM ones and defining $\mathcal{R}_{K^{(*)}}^\nu \equiv \mathcal{B}(B \to K^{(*)}\nu\bar{\nu})/\mathcal{B}(B \to K^{(*)}\nu\bar{\nu})_{\mathrm{SM}}$, we obtain

$$\mathcal{R}_K^\nu = \mathcal{R}_{K^*}^\nu = \frac{2}{3} + \frac{1}{3}\left|\frac{C_L^{\mathrm{SM}} + C_L^{\mathrm{NP}}}{C_L^{\mathrm{SM}}}\right|^2. \qquad (11)$$

Combining the charged and neutral B meson decays, the tightest limits [90] are set by Belle [91], who find

$$\mathcal{R}_K^\nu < 3.9, \qquad \mathcal{R}_{K^*}^\nu < 2.7 \qquad (12)$$

at the 90% confidence level (C.L.). The tighter constraint comes from $\mathcal{R}_{K^*}^\nu$, and is shown by the cyan lines in Fig. 1. The allowed region fully contains the blue hyperbolas favored by $b \to s\ell\ell$.

The $Z'bs$ and $Z'bb$ couplings induce Z' production at LHC via $b\bar{s} \to Z'$ and $b\bar{b} \to Z'$. Hence, with $Z' \to \mu^+\mu^-$, these couplings are constrained by dimuon resonance searches at the LHC.

We use the results from ATLAS, performed with 36.1 fb^{-1} at 13 TeV [92] and extract [93] the 95% credibility level limit: $\sigma(pp \to Z' + X)\mathcal{B}(Z' \to \mu^+\mu^-) <$ 42 fb (9 fb) for $m_{Z'} = 200$ GeV (500 GeV). We calculate the Z' production cross section at leading order (LO) using MadGraph5_aMC@NLO [94] with the NN23LO1 parton distribution function (PDF) set [95]. As the ATLAS search does not veto additional activity in the event, we include also the processes $gs \to Z'b$, $gb \to Z'b$ and $gg \to Z'b\bar{b}, Z'b\bar{s}$ in the cross-section calculation. We defer the more detailed discussion about Z' production at the LHC to Sec. IV. From the cross sections and the ATLAS limits, we find

$$\sqrt{|g_{bs}^L|^2 + 0.33|g_{bb}^L|^2} < 0.004 \quad (m_{Z'} = 200 \text{ GeV}),$$

$$\sqrt{|g_{bs}^L|^2 + 0.21|g_{bb}^L|^2} < 0.011 \quad (m_{Z'} = 500 \text{ GeV}) \qquad (13)$$

in scenario (i). In scenario (ii), where the Z' couples to the LH muon current, the limits are weakened by an overall factor of $2/\sqrt{3}$ on the right-hand side due to the change in $\mathcal{B}(Z' \to \mu^+\mu^-)$.

As long as $|g_{bb}^L| \lesssim |g_{bs}^L|$, which is our scenario of interest, these limits are significantly weaker than those from the $B_s - \bar{B}_s$ mixing. Hence, they are not shown in Fig. 1. For flavor universal models, Z' masses below $m_{Z'} \lesssim 3\text{–}4.5$ TeV are ruled out by Ref. [92] with 95% C.L. However, a very weakly coupled and flavor nonuniversal light Z' such as described by Eq. (1) escapes the detection and could emerge in the future runs of the LHC.

Muon pair production in the scattering of a muon neutrino and a nucleus N, known as neutrino trident production, tightly constrains $Z'\mu\mu$ and $Z'\nu_\mu\nu_\mu$ couplings [96]. The ratio between the total $\nu_\mu N \to \nu_\mu N\mu^+\mu^-$ cross section and its SM prediction is given by [31]

$$\frac{\sigma}{\sigma^{\mathrm{SM}}} = \frac{1 + [1 + 4s_W^2 + 2(g_{\mu\mu}^V)^2 \frac{v^2}{m_{Z'}^2}]^2}{1 + (1 + 4s_W^2)^2}, \qquad (14)$$

in scenario (i) with $m_{Z'} \gtrsim 10$ GeV. The measurement [97] by the CCFR collaboration is in a good agreement with the SM, and implies $\sigma/\sigma^{\mathrm{SM}} = 0.82 \pm 0.28$. We show the resulting 2σ upper limits on $|g_{\mu\mu}^V|$ by the horizontal solid red lines in Fig. 1.

The couplings of the Z boson with the muon and muon neutrino are modified by Z'-loop contributions, which can lead to violation of the lepton-flavor universality in Z decays. In scenario (i), the vector and axial-vector $Z\mu\mu$ couplings relative to the SM-like Zee couplings are given by [31,50]

$$\frac{g_{V\mu}}{g_{Ve}} \simeq \frac{g_{A\mu}}{g_{Ae}} \simeq 1 + \frac{(g_{\mu\mu}^V)^2}{16\pi^2} \mathrm{Re}[\mathcal{K}(m_Z^2/m_{Z'}^2)], \qquad (15)$$

where $\mathcal{K}(m_Z^2/m_{Z'}^2)$ is a loop function given in Ref. [98], and its real part is taken to match the convention of Ref. [99]. Here, the lepton-flavor universality in the SM case is exploited. Similarly, normalized $Z\nu\nu$ couplings are given by

$$\frac{g_{V\nu}}{g_{Ae}} = \frac{g_{A\nu}}{g_{Ae}} \simeq -\left\{1 + \frac{1}{3}\frac{(g_{\mu\mu}^L)^2}{16\pi^2}\mathrm{Re}[\mathcal{K}(m_Z^2/m_{Z'}^2)]\right\}, \qquad (16)$$

where the factor of 1/3 effectively takes into account the fact that only $Z \to \nu_\mu\bar{\nu}_\mu$ is affected by the Z' among the three neutrino modes.

The Z couplings were very precisely measured at SLC and LEP. Relevant results from the average of 14 electroweak (EW) measurements are $g_{Ve} = -0.03816 \pm 0.00047$, $g_{Ae} = -0.50111 \pm 0.00035$, $g_{V\mu} = -0.0367 \pm 0.0023$, $g_{A\mu} = -0.50120 \pm 0.00054$ and $g_{V\nu} = g_{A\nu} = 0.5003 \pm 0.0012$ [99]. Of the four possible Z coupling ratios, we take only the one which is most sensitive to the effect of the Z', i.e., $g_{A\mu}/g_{Ae} = 1.00018 \pm 0.00128$, where the uncertainties are added in quadrature. The resulting 2σ upper limits on $|g_{\mu\mu}^V|$ are shown by the horizontal red dashed lines in Fig. 1.

Nonzero values of g_{bs}^L or g_{bb}^L can alter the Zbb and Zss couplings at one loop. Taking the b and s quarks to be massless, we find that the Z' loop with a nonzero g_{bs}^L modifies the LH Zbb and Zss couplings g_{Lb} and g_{Ls} relative to their SM values g_{Lb}^{SM} and g_{Ls}^{SM} in the same way as the LH $Z\mu\mu$ coupling, but with the replacement $g_{\mu\mu}^L \to g_{bs}^L$:

$$\frac{g_{Lb}}{g_{Lb}^{\mathrm{SM}}} \simeq \frac{g_{Ls}}{g_{Ls}^{\mathrm{SM}}} \simeq 1 + \frac{(g_{bs}^L)^2}{16\pi^2}\mathrm{Re}[\mathcal{K}(m_Z^2/m_{Z'}^2)]. \qquad (17)$$

The RH counterparts remain unchanged. The effect of the Z' loop can be constrained by comparing the measured

value $g_{Lb} = -0.4182 \pm 0.0015$ $(g_{Ls} = -0.423 \pm 0.012)$ [99] to the corresponding SM prediction $g_{Lb}^{SM} = -0.42114^{+0.00045}_{-0.00024}$ ($g_{Ls}^{SM} = -0.42434^{+0.00018}_{-0.00016}$), derived from the SM Z-pole fit [99]. Since g_{Lb} is more precisely measured than g_{Ls},[2] we use g_{Lb} to extract the limit on g_{bs}^{L}. Adding the errors in g_{Lb} and g_{Lb}^{SM} in quadrature after symmetrizing the g_{Lb}^{SM} errors, we find the 2σ upper limit $|g_{bs}^{L}| \lesssim 0.34(0.67)$ for $m_{Z'} = 200$ (500) GeV. These limits are much weaker than the ones obtained from the B_s mixing, and we do not display them in Fig. 1. A similar conclusion can be made for the g_{bb}^{L} coupling as well.

If both g_{bs}^{L} and g_{bb}^{L} are nonzero, an FCNC decay $Z \to b\bar{s}$, which is absent in the SM at tree level, is induced by the one-loop Z' contribution. A preliminary result by DELPHI [100] sets the 90% C.L. upper limit $R_{b\ell} = \sum_{q=d,s}\sigma(e^+ e^- \to b\bar{q} + \bar{b}q)/\sigma(e^+ e^- \to \text{hadrons}) \leq 2.6 \times 10^{-3}$ at the energy scale of the Z mass. Using $\mathcal{B}(Z \to \text{hadrons}) \simeq 70\%$ [80], one may rewrite the limit as $\sum_{q=d,s}\mathcal{B}(Z \to b\bar{q} + \bar{b}q) \lesssim 1.8 \times 10^{-3}$. Since the Z'-loop-induced LH Zbs coupling is suppressed by the factor $g_{bs}^{L}g_{bb}^{L}/(16\pi^2)$, the DELPHI limit is relevant only if both g_{bs}^{L} and g_{bb}^{L} are $\mathcal{O}(1)$ and the Z' mass is not far from the Z mass. Since the B_s-mixing constraint on g_{bs}^{L} is much tighter, and we concentrate on the case $|g_{bb}^{L}| \lesssim |g_{bs}^{L}|$, the impact on $\mathcal{B}(Z \to b\bar{s} + \bar{b}s)$ is generically far below the DELPHI limit in the scenarios considered in this paper.

The Z' one-loop contribution to the muon anomalous magnetic moment $a_\mu = (g_\mu - 2)/2$ is [101]

$$\Delta a_\mu = \frac{(g_{\mu\mu}^{V})^2}{12\pi^2}\frac{m_\mu^2}{m_{Z'}^2}, \tag{18}$$

where scenario (i) and $m_{Z'} \gg m_\mu$ are assumed. The difference between the measured value of a_μ and its SM prediction is $(2.9 \pm 0.9) \times 10^{-9}$ [102]. Assigning this difference to Eq. (18) yields the dark yellow 2σ regions in Fig. 1. Since the 2σ constraints from the neutrino trident cross section are tighter, the Z' does not solve the tension in the muon $g - 2$. At the 3σ level, the $g_\mu - 2$ regions become compatible with the neutrino trident production constraints. Therefore, we ignore $g_\mu - 2$ in the rest of this paper.

We have discussed so far the constraints in scenario (i), summarized in Fig. 1 on the $g_{\mu\mu}^{V}$ vs g_{bs}^{L} plane. From Fig. 1, we find the constraint on g_{bs}^{L} is very stringent due to the $B_s - \bar{B}_s$ mixing, while the constraint on $g_{\mu\mu}^{V}$ is much weaker. With the 30% NP effects allowed in the $B_s - \bar{B}_s$ mixing amplitude, the former constraint is $|g_{bs}^{L}| \lesssim 1.4(3.6) \times 10^{-3}$ for $m_{Z'} = 200(500)$ GeV, imposing the

lower limit on the $Z'\mu\mu$ coupling $|g_{\mu\mu}^{V}| \gtrsim 0.031(0.078)$ on the $b \to s\ell\ell$ hyperbolas. This validates the numerical values of the branching ratios in Eq. (7) to a good approximation, if $|g_{bb}^{L}|$ is not too large compared to $|g_{bs}^{L}|$.

The qualitative feature is the same in scenario (ii), where the $Z'\mu\mu$ coupling is of LH, as the $B_s - \bar{B}_s$ mixing constraint does not change. Some of the other observables would give slightly different constraints on the $Z'\mu\mu$ coupling, but the effect is minor to our study. The only notable difference from scenario (i) is the slight change in the value of $\mathcal{B}(Z' \to \mu^+\mu^-)$ from Eq. (7). A nonzero axial-vector $Z'\mu\mu$ coupling can make $B_s \to \mu^+\mu^-$ relevant, but the latest LHCb result [103] does not exclude the allowed regions for the $b \to s\ell\ell$ anomalies.

IV. DISCOVERY AND IDENTIFICATION OF THE Z' AT THE LHC

Having determined the constraints on the Z' couplings, we proceed to study signatures for direct production of the on-shell Z' in pp collisions with a center-of-mass energy of $\sqrt{s} = 14$ TeV. The goal of this study is to ascertain the LHC potential for both discovery of the Z' and determination of the flavor structure of its couplings. Therefore, motivated by the tensions in $b \to s\ell\ell$, we focus on the role of the $Z'bs$ coupling g_{bs}^{L}. If this is the dominant coupling to the quark sector, the Z' will be primarily produced via the parton-level process $b\bar{s} \to Z'$ shown in Fig. 2. With the decay $Z' \to \mu^+\mu^-$, the Z' may be discovered in the conventional dimuon resonance searches.

Such a discovery of a dimuon resonance, however, does not necessarily imply the existence of the $Z'bs$ coupling. In general, the process $pp \to Z' + X$ may be facilitated by coupling to other quarks, particularly flavor-diagonal couplings. To test for dominance of the $Z'bs$ coupling, we propose to also search for $pp \to Z'b + X$ (see Fig. 3 for typical parton-level processes). A $Z'bb$ coupling, predicted in many models (e.g., Refs. [31,51,58,61]), motivated by the $b \to s\ell\ell$ anomalies, also contributes to $pp \to Z' + X$ and $pp \to Z'b + X$ via the parton-level processes $b\bar{b} \to Z'$ and $gb \to Z'b$. Since a $Z'bb$ coupling also leads to $pp \to b\bar{b}Z' + X$, via, for example, $gg \to Z'b\bar{b}$, measuring the cross section for $pp \to Z'b\bar{b} + X$ may facilitate discriminating the $Z'bb$ coupling from $Z'bs$. Similarly, the production process $pp \to Z'b\bar{s} + X$, occurring due to $gg \to Z'b\bar{s}$, can in principle help probe the $Z'bs$ coupling.
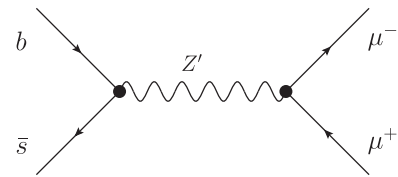
FIG. 2.   A Feynman diagram for the process $b\bar{s} \to Z' \to \mu^+\mu^-$.

---

[2]Furthermore, the measured value of g_{Ls} in Ref. [99] is obtained under the assumption of $g_{Ls} = g_{Ld}$. This is not valid in our case, since g_{Ld} receives no correction from Z' at one loop.
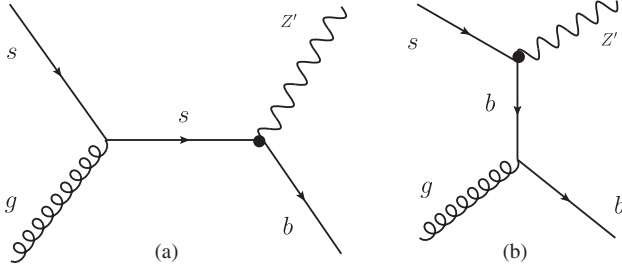
FIG. 3.   Feynman diagrams for $gs \to Z'b$.

We explore these signatures using the effective Lagrangian of Eq. (1) with scenario (i), i.e., with a vector $Z'\mu\mu$ coupling. For each of the two Z'-mass values studied, we fix the couplings to the benchmark points shown by the red dots in Fig. 1,

$$|g_{bs}^L| = 0.001, \quad |g_{\mu\mu}^V| = 0.04 \quad (m_{Z'} = 200 \text{ GeV}),$$
$$|g_{bs}^L| = 0.0025, \quad |g_{\mu\mu}^V| = 0.1 \quad (m_{Z'} = 500 \text{ GeV}). \quad (19)$$

These values are selected such that g_{bs}^L leads to a 15% enhancement in the $B_s - \bar{B}_s$-mixing amplitude M_{12}. The value of $g_{\mu\mu}^V$ is then chosen so as to lie in the range given by Eqs. (5) and (3). We note that one may take a larger $|g_{bs}^L|$ (with a smaller $|g_{\mu\mu}^V|$), which would enlarge the $pp \to Z' + X$ and $pp \to Z'b + X$ cross sections by up to a factor of 2, with the $B_s - \bar{B}_s$-mixing constraint saturated at 2σ, i.e., a ∼30% enhancement in M_{12}.

For the $Z'bb$ coupling, we study three cases for each benchmark point. The baseline case is $g_{bb}^L = 0$, which restricts assumptions about the Z' couplings to the minimum needed to explain the $b \to s\ell\ell$ anomalies. In addition, we also explore the cases $g_{bb}^L = g_{bs}^L$ and $g_{bb}^L = 2g_{bs}^L$, to study the impact of a nonzero g_{bb}^L. These choices of quark couplings satisfy the dimuon resonance search limits in Eq. (13) and maintain the Z' branching ratios in Eq. (7).

In the following subsections, we mainly focus on the discovery potential of the Z' in the production processes $pp \to Z' + X$, $pp \to Z'b + X$, and $pp \to Z'b\bar{b} + X$, with the Z' always decaying to $\mu^+\mu^-$. We use Monte Carlo event generator MadGraph5_aMC@NLO [94] to generate signal and background samples at LO with the NN23LO1 PDF set [95]. The effective Lagrangian of Eq. (1) is implemented in the FeynRules 2.0 [104] framework. The matrix elements for signal and background are generated with up to two additional jets and interfaced with PYTHIA 6.4 [105] for parton showering and hadronization. Matching is performed with the MLM prescription [106]. The generated events are passed into the Delphes 3.3.3 [107] fast detector simulation to incorporate detector effects based on ATLAS.

A. Observation of $pp \to Z' + X$

Several SM processes constitute background for $pp \to Z' + X$, where we remind the reader that the Z'

decays into $\mu^+\mu^-$. The dominant background is due to the Drell-Yan (DY) events, $pp \to Z/\gamma^* + X$. The process $pp \to t\bar{t}$ event with semileptonic decay of both top quarks is the next largest background. Smaller backgrounds arise from $pp \to Wt$ and VV, where $V \equiv W, Z$. Background may also arise from leptons produced in heavy-flavor decays or from jets faking leptons. These background sources are not well modeled by the simulation tools, and we ignore them, assuming that they can be reduced to subdominant level with lepton quality cuts without drastically impacting the results of our analysis.

We scale the LO cross sections obtained by MadGraph5_aMC@NLO as follows. The DY cross section is normalized to a next-to-next-to-leading order (NNLO) QCD + NLO EW cross section by a factor of 1.27, obtained with FEWZ 3.1 [108] in the dimuon-invariant mass range $m_{\mu\mu} > 106$ GeV. We normalize the LO $pp \to t\bar{t}$ and $pp \to Wt$ cross sections to NNLO + NNLL cross sections by 1.84 [109] and 1.35 [110], respectively. The $pp \to WW$, $pp \to WZ$ and $pp \to ZZ$ cross sections are normalized to NNLO QCD by 1.98 [111], 2.07 [112] and 1.74 [113], respectively. We do not apply correction factors to the signal cross sections throughout this paper.

We select events that contain at least two oppositely charged muons. The transverse momentum of each muon is required to satisfy $p_\mu^T > 50$ GeV, and its pseudorapidity must be in the range $|\eta_\mu| < 2.5$. The two muons must satisfy $\Delta R_{\mu\mu} = \sqrt{\Delta\phi_{\mu\mu}^2 + \Delta\eta_{\mu\mu}^2} > 0.4$, where $\Delta\phi_{\mu\mu}$ and $\Delta\eta_{\mu\mu}$ are the separations in azimuthal angle and pseudorapidity between the muons. Finally, we require the invariant mass of the two muons to satisfy $|m_{\mu\mu} - m_{Z'}| < m_{\text{cut}}$, where $m_{\text{cut}} = 4$ GeV and 16 GeV for $m_{Z'} = 200$ GeV and $m_{Z'} = 500$ GeV, respectively. These values are chosen so as to maximize the naive local significance of the no-signal hypothesis, $S_l = N_S/\sqrt{N_B}$, where N_S and N_B are the expected signal and background yields.

The invariant mass cut $|m_{\mu\mu} - m_{Z'}| < m_{\text{cut}}$ is not realistic for a discovery scenario, in which one does not know the true mass $m_{Z'}$. However, the value of S_l thus obtained is a rough estimate of the one that will be found by the more sophisticated analysis that will eventually be performed with the full LHC data. One is actually interested in the global significance S_g, which accounts for the probability to obtain the given value of S_l anywhere in the dimuon-invariant mass range. Rigorous methods for estimating S_g exist [114]. However, at this level of approximation, it is sufficient to use the crude estimate

$$P_g = P_l \frac{m_{\text{cut}}}{m_{\text{range}}}, \quad (20)$$

where P_g and P_l are the χ^2 probabilities corresponding to S_g and S_l, respectively, and m_{range} is the size of the range of $m_{\mu\mu}$ values explored in the analysis. Since cross sections

TABLE I. Cross sections for the signal process $pp \to Z' + X$ with $Z' \to \mu^+\mu^-$, and the dominant backgrounds after the event selection for the benchmark points defined in Eq. (19) with the three choices for g_{bb}^L. The combined cross sections for WW, WZ and ZZ backgrounds are denoted together as VV.

	σ_{signal} (fb)			$\sigma_{\text{background}}$ (fb)			
$m_{Z'}$ (GeV)	$g_{bb}^L = 0$	$g_{bb}^L = g_{bs}^L$	$g_{bb}^L = 2g_{bs}^L$	DY	$t\bar{t}$	Wt	VV
200	1.0	1.3	2.2	170	41	4.1	5.1
500	0.27	0.33	0.50	14	4.3	0.5	1.0

TABLE II. Local significance $S_l = N_S/\sqrt{N_B}$ for discovery of the process $pp \to Z' + X$ with $Z' \to \mu^+\mu^-$, with an integrated luminosity of 3000 fb^{-1}, given the signal and background cross sections shown in Table I.

	Local significance		
$m_{Z'}$ (GeV)	$g_{bb}^L = 0$	$g_{bb}^L = g_{bs}^L$	$g_{bb}^L = 2g_{bs}^L$
200	3.7	4.9	8.3
500	3.3	4.1	6.5

drop to negligible levels at high $m_{\mu\mu}$, it is reasonable to take $m_{\mu\mu} \sim 2\text{–}3$ TeV for this estimate.

The cross sections for signal and backgrounds after the cuts are listed in Table I for the benchmark points defined in Eq. (19) with the three choices of g_{bb}^L. The corresponding values of the local significance S_l for an integrated luminosity $L = 3000$ fb^{-1} are summarized in Table II. Inserting the values of S_l into Eq. (20), we conclude that the global significance will likely be greater than 5σ for the case $g_{bb}^L = 2g_{bs}^L$, allowing separate discovery by ATLAS and CMS. For $|g_{bb}^L| \leq |g_{bs}^L|$, the global significance is under 5σ. Whether the 5σ mark will be passed by combining ATLAS and CMS results is beyond the precision of our rough estimate.

A larger $|g_{bs}^L|$ can enhance the significance in each benchmark scenario. For the scenario of $m_{Z'} = 200(500)$ GeV with $g_{bb}^L = 0$, taking $|g_{bs}^L| = 0.0013(0.0034)$ with $|g_{\mu\mu}^V| = 0.031(0.074)$ pushes the local significance slightly above 6σ, which may imply a global significance of 5σ. In this case, the $B_s - \bar{B}_s$ mixing amplitude $|M_{12}|$ is also enhanced from the SM one by 25% (28%), but still within the nominal 2σ allowed range, as discussed in Sec. III.

B. Observation of $pp \to Z'b + X$

The main SM background for $pp \to Z'b + X$ is $pp \to t\bar{t}$. The second-largest background is Drell Yan with at least one additional b jet, labeled as DY $+ b$. Smaller contributions arise from DY $+ c$, $pp \to Wt$, $pp \to VV$, and DY $+ j$, where j stands for a jet from a gluon or a u, d, or s quark. We normalize the cross sections for DY $+ b$, DY $+ c$, and DY $+ j$ to NNLO QCD by 1.83 [115]. The correction factors for $pp \to t\bar{t}$, $pp \to Wt$, and $pp \to VV$ are taken to be the same as in Sec. IV A.

We select simulated events that contain at least two opposite-charge muons. The muons are required to be in the pseudorapidity range $|\eta_\mu| < 2.5$, have minimal transverse momenta of $p_\mu^T > 50(60)$ GeV for $m_{Z'} = 200(500)$ GeV, and be separated by $\Delta R_{\mu\mu} > 0.4$. Jets are reconstructed using the anti-k_T algorithm with radius parameter $R = 0.5$. It is assumed that a b-tagging algorithm reduces the efficiency for c jets and light jets by factors of 5 and 137, respectively [116]. Its efficiency for b jets is calculated in Delphes, accounting for the p_T and η dependence. The leading b jet is required to have transverse momentum $p_b^T > 30$ GeV with $|\eta_b| < 2.5$, and its separation from each of the two leading muons must satisfy $\Delta R_{b\mu} > 0.4$. We reject events that have a second b-tagged jet with $p_b^T > 30$ GeV, slightly increasing the local significance. The missing transverse energy must be less than 40 GeV, in order to reduce $pp \to t\bar{t}$ and $pp \to Wt$ backgrounds. Finally, we apply the optimized dimuon-invariant mass cut $|m_{\mu\mu} - m_{Z'}| < 5(15)$ GeV for $m_{Z'} = 200(500)$ GeV.

The resulting cross sections are shown in Table III, and the corresponding local signal significances with 3000 fb^{-1} are summarized in Table IV. The local significances are slightly smaller than the corresponding ones in Table II, except in the case of $m_{Z'} = 500$ GeV and $g_{bb} = 2g_{bs}^L$. Thus, we conclude that, like $pp \to Z' + X$, the process $pp \to Z'b + X$ is likely be discovered at $S_g > 5$ if $g_{bb}^L \geq 2g_{bs}^L$ in our benchmark points. By scaling the values in Table IV, we observe that a local significance of 6σ can be attained with $|g_{bs}^L| \gtrsim 0.0014(0.0036)$ for $m_{Z'} = 200(500)$ GeV, even if $g_{bb}^L = 0$, at the cost of a $\sim30\%$ enhancement in $|M_{12}/M_{12}^{\text{SM}}|$.

C. Observation of $pp \to Z'b\bar{b} + X$ and $pp \to Z'b\bar{s} + X$

The dominant SM backgrounds for $pp \to Z'b\bar{b} + X$ are $pp \to t\bar{t}$, $pp \to Wt$ and DY $+ b$ or c jets. $pp \to VV$ gives a negligible contribution. We adopt the same correction

TABLE III. Cross sections for the signal process $pp \to Z'b + X$ with $Z' \to \mu^+\mu^-$, and the dominant backgrounds after the event selection for the benchmark points defined in Eq. (19) with the three choices for g_{bb}^L.

	σ_{signal} (fb)			$\sigma_{\text{background}}$ (fb)					
$m_{Z'}$ (GeV)	$g_{bb}^L = 0$	$g_{bb}^L = g_{bs}^L$	$g_{bb}^L = 2g_{bs}^L$	DY $+ b$	DY $+ c$	DY $+ j$	$t\bar{t}$	Wt	VV
200	0.17	0.22	0.37	1.3	1.0	0.22	5.6	0.8	0.5
500	0.043	0.049	0.10	0.15	0.048	0.028	0.26	0.08	0.064

TABLE IV.   Local significance $S_l = N_S/\sqrt{N_B}$ for discovery of the process $pp \to Z'b + X$ with $Z' \to \mu^+\mu^-$, with an integrated luminosity of 3000 fb^{-1}, given the signal and background cross sections shown in Table III.

$m_{Z'}$ (GeV)	Local significance		
	$g_{bb}^L = 0$	$g_{bb}^L = g_{bs}^L$	$g_{bb}^L = 2g_{bs}^L$
200	3.0	3.9	6.6
500	3.0	3.4	7.2

TABLE V.   Cross sections for the signal process $pp \to Z'b\bar{b} + X$ with $Z' \to \mu^+\mu^-$, and the dominant backgrounds after the event selection for the benchmark points defined in Eq. (19) with the three choices for g_{bb}^L.

$m_{Z'}$ (GeV)	σ_{signal} (fb)			$\sigma_{\text{background}}$ (fb)		
	$g_{bb}^L = 0$	$g_{bb}^L = g_{bs}^L$	$g_{bb}^L = 2g_{bs}^L$	DY +h.f. jets	$t\bar{t}$	Wt
200	0.00018	0.0025	0.0094	0.2	1.5	0.5
500	0.00008	0.0006	0.0026	0.07	0.27	0.17

factors for the background cross sections and follow the same event selection criteria as in Sec. IV C, and in addition require the subleading b jet to have $p_b^T > 30$ GeV, $|\eta_b| < 2.5$, and to be separated from the leading b jet and each of the two leading muons by $\Delta R > 0.4$, for both the Z' masses.

The resulting cross sections are shown in Table V. The $g_{bb}^L = 0$ cases have tiny but nonzero cross sections, due to production via $b\bar{s} \to Z'g^*$, with $g^* \to b\bar{b}$. By contrast, a nonzero g_{bb}^L induces the less suppressed process $gg \to Z'b\bar{b}$. The corresponding local signal significances for 3000 fb^{-1} are given in Table VI. As the local significances are much less than 1, we conclude that observation of this process is not possible at the LHC within the range of couplings explored here.

In general, $|g_{bb}^L|$ may take a larger value, up to the limit of Eq. (13), namely, $|g_{bb}^L| = 0.007$ (0.024) for $m_{Z'} = 200$ (500) GeV with $g_{bs}^L \sim 0$. With these values, we estimate the cross section of $pp \to Z'b\bar{b} + X$ to be 0.098 fb (0.055 fb) after the event selection cuts. This corresponds

TABLE VI.   Local significance $S_l = N_S/\sqrt{N_B}$ for discovery of the process $pp \to Z'b\bar{b} + X$ with $Z' \to \mu^+\mu^-$, with an integrated luminosity of 3000 fb^{-1}, given the signal and background cross sections shown in Table V.

$m_{Z'}$ (GeV)	Local significance		
	$g_{bb}^L = 0$	$g_{bb}^L = g_{bs}^L$	$g_{bb}^L = 2g_{bs}^L$
200	0.007	0.1	0.35
500	0.006	0.05	0.2

to a local significance of around 3.6σ (4.1σ) for an integrated luminosity of 3000 fb^{-1}. Thus, a global significance of 5σ is not likely. We note, however, that since we used the same QCD correction factors for the background cross sections as in the $pp \to Z'b + X$ case, there is a greater uncertainty on these cross sections.

Generally, the cross section for $pp \to Z'b\bar{b} + X$ is strongly suppressed by the three-body phase space. Since the same suppression applies for $pp \to Z'b\bar{s} + X$, one expects the cross section for this process to be small as well. Moreover, the process $pp \to Z'b\bar{s} + X$ would also suffer from light-jet backgrounds which make the discovery not possible, given the $B_s - \bar{B}_s$ mixing constraint.

V. IMPACT OF THE RIGHT-HANDED $Z'bs$ COUPLING

In this section, we study an impact of a tiny but nonzero RH $Z'bs$ coupling by adding the following terms to the effective Lagrangian in Eq. (1):

$$\Delta\mathcal{L} = -g_{bs}^R(\bar{b}\gamma^\alpha P_R s + \bar{s}\gamma^\alpha P_R b)Z'_\alpha. \qquad (21)$$

The resulting additional contributions to $b \to s\mu^+\mu^-$ are described by effective operators as in Eq. (2), with P_L replaced by P_R, and with C_9^{NP} and C_{10}^{NP} replaced by the Wilson coefficients

$$C_9' = \frac{g_{bs}^R g_{\mu\mu}^V}{\mathcal{N}m_{Z'}^2}, \qquad C_{10}' = \frac{g_{bs}^R g_{\mu\mu}^A}{\mathcal{N}m_{Z'}^2}. \qquad (22)$$

There is no significant indication for nonzero $C'_{9,10}$ in the majority of the $b \to s\ell\ell$ global-fit analyses. However, even a tiny g_{bs}^R can drastically affect the $B_s - \bar{B}_s$ mixing, which is now given by [31]

$$\frac{M_{12}}{M_{12}^{\text{SM}}} = 1 + \frac{1}{m_{Z'}^2}[(g_{bs}^L)^2 - 9.7g_{bs}^L g_{bs}^R + (g_{bs}^R)^2]$$
$$\times \left(\frac{g_2^2}{16\pi^2 v^2}(V_{tb}V_{ts}^*)^2 S_0\right)^{-1}, \qquad (23)$$

calculated with the hadronic matrix elements in Ref. [117]. The large negative coefficient of the $g_{bs}^L g_{bs}^R$ term, which is partly due to renormalization group effects [79], means that a small value of g_{bs}^R allows for a large g_{bs}^L, due to cancellation between the terms. In Fig. 4 we show the $B_s - \bar{B}_s$-mixing constraint on g_{bs}^R vs g_{bs}^L, when $|M_{12}|$ is allowed to change by up to 30% of its SM value. Reducing the allowed NP contribution to $|M_{12}|$, say, to 15%, would narrow the width of the tilted-cross-shaped allowed region in Fig. 4. However, it would not change the conclusion, namely, that a large value of $|g_{bs}^L|$ is allowed. What now becomes the most significant limit on g_{bs}^L is the ATLAS
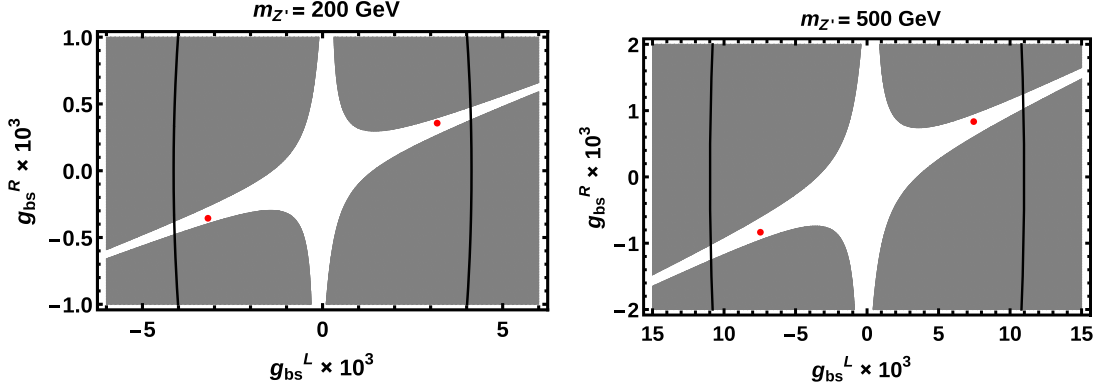
FIG. 4. Constraints on g_{sb}^R vs g_{sb}^L (in units of 10^{-3}) for $m_{Z'} = 200$ GeV (left) and 500 GeV (right), when allowing the $B_s - \bar{B}_s$-mixing amplitude to deviate by up to 30% from its SM prediction. The gray regions are excluded. The solid lines show the exclusion by the ATLAS dimuon resonance search [92] for $\mathcal{B}(Z' \to \mu^+\mu^-) \simeq 2/3$. The red dots show our benchmark points.

dimuon resonance search [92], shown by the solid lines, assuming Eq. (7).

The cancellation in M_{12} requires $g_{bs}^L g_{bs}^R > 0$. This implies $(\mathrm{Re}C_9^{\mathrm{NP}})(\mathrm{Re}C_9') > 0$, contrary to the best-fit values for C_9^{NP} and C_9', e.g., Refs. [15,16]. However, the cancellation requires only $g_{bs}^R \sim 0.1 g_{bs}^L$ or $C_9' \sim 0.1 C_9^{\mathrm{NP}}$. While the fits favor $C_9^{\mathrm{NP}} \sim -1$ and are consistent with $C_9' = 0$, they cannot exclude a small negative C_9'. Indeed, the point $(C_9^{\mathrm{NP}}, C_9') = (-1.11, -0.1)$ is at the border of the 1σ ellipse in Ref. [15] with the assumption $C_{10}^{\mathrm{NP}} = C_{10}' = 0$.

To illustrate the impact of such a possibly large $Z'bs$ coupling on the Z' discovery potential, we consider scenario (i) with the following benchmark points for $m_{Z'} = 200$ and 500 GeV respectively (corresponding to the dots in Fig. 4):

$$|g_{bs}^L| = 0.0032, \quad |g_{bs}^R| = 0.00036, \quad |g_{\mu\mu}^V| = 0.012,$$
$$|g_{bs}^L| = 0.0075, \quad |g_{bs}^R| = 0.00083, \quad |g_{\mu\mu}^V| = 0.032.$$
$$(24)$$

Both points correspond to $(C_9^{\mathrm{NP}}, C_9') = (-1.11, -0.1)$. The effects of the tiny g_{bs}^R on other constraints, e.g., $B \to K^{(*)}\nu\bar{\nu}$, are negligible. Taking $g_{bb}^L = 0$, we find that the $pp \to Z' + X$ and $pp \to Z'b + X$ cross sections are

TABLE VII. Local significance $N_S/\sqrt{N_B}$ for discovery of the process $pp \to Z' + X \to \mu^+\mu^- + X$ and $pp \to Z'b + X \to \mu^+\mu^- b + X$ with the integrated luminosity of 300 fb^{-1}, obtained by rescaling the results of Tables II and IV to the benchmark points defined in Eq. (24) for $g_{bb}^L = 0$.

	Local significance	
$m_{Z'}$ (GeV)	$\mu^+\mu^- + X$	$\mu^+\mu^- b + X$
200	9.3	7.6
500	7.7	6.9

highly enhanced compared to the ones in Sec. IV, while the relatively large g_{bs}^L values lead to a non-negligible $Z' \to b\bar{s}$ branching ratio, slightly reducing $\mathcal{B}(Z' \to \mu^+\mu^-)$ from $\sim 66\%$ to $\sim 52\%$ and $\sim 55\%$ respectively for 200 and 500 GeV Z'.

Taking account of these effects and rescaling the significances obtained in Sec. IV, we show in Table VII the local significances for discovery of $pp \to Z' + X$ and $pp \to Z'b + X$ with the integrated luminosity of 300 fb^{-1}, for the two benchmark points defined above. The results suggest that both processes can be discovered with the Run-3 data set, even if the $Z'bb$ coupling vanishes. A larger $|g_{bs}^L|$ in this scenario enhances the cross section for the $pp \to Z'b\bar{s} + X$ process, but the discovery would still be beyond the reach of the HL-LHC.

VI. SUMMARY AND DISCUSSIONS

Observed tensions in $b \to s\ell\ell$ measurements can be explained by a new Z' boson that couples to the left-handed $b \to s$ current as well as to muons. In this paper, we have studied the collider phenomenology of such a Z' based on an effective model introduced in Eq. (1). For this purpose, we first estimated phenomenological constraints on the $Z'bs$ and $Z'\mu\mu$ couplings for the representative masses $m_{Z'} = 200$ and 500 GeV. The most important constraint is the B_s mixing, which tightly constrains the LH $Z'bs$ coupling g_{bs}^L. For fixed values of g_{bs}^L and $m_{Z'}$, the allowed coupling to muons is determined by global fits to $b \to s\ell\ell$ data, up to the value allowed by the constraint from the neutrino trident production, where the $Z'\nu_\mu\nu_\mu$ coupling is related to $Z'\mu\mu$ coupling by the $SU(2)_L$ symmetry. We also introduced the $Z'bb$ coupling g_{bb}^L, which is mildly constrained by the dimuon resonance search at the LHC. The resulting couplings are such that the Z' decays mostly to $\mu^+\mu^-$ and $\nu_\mu\bar{\nu}_\mu$, with the two branching ratio values mildly depending on whether the muon coupling is vectorlike or left-handed.

Given the coupling constraints, we explored the capability of the 14 TeV LHC to discover the Z' and to determine the flavor structure of its couplings. For the sake of this dual goal, we studied the two processes $pp \to Z' + X \to \mu^+\mu^- + X$ and $pp \to Z'b + X \to \mu^+\mu^- b + X$, where the former may be induced by $b\bar{s} \to Z'$ and/or $b\bar{b} \to Z'$ and the latter by $gs \to Z'b$ and/or $gb \to Z'b$. We considered two representative Z' masses of 200 and 500 GeV with three scenarios for the $Z'bb$ coupling $g_{bb}^L = 0$, g_{bs}^L or $2g_{bs}^L$. For $g_{bb}^L = 0$, we found that discovery of $pp \to Z' + X$ and $pp \to Z'b + X$ (with about 5σ global significance) with 3000 fb^{-1} data requires a large $Z'bs$ coupling, so that the B_s mixing amplitude M_{12} is enhanced by $\sim 30\%$ or more relative to the SM expectation. This corresponds roughly to the 2σ upper limits of the global analyses [83,84] for the CKM parameters. With a nonzero g_{bb}^L, discovery in both the modes is possible without such a drastic effect on the B_s mixing; in particular, for $g_{bb}^L = 2g_{bs}^L$, discovery is possible with a $\sim 15\%$ deviation in the M_{12}. For further discrimination between the $Z'bs$ and $Z'bb$ couplings, we also studied the process $pp \to Z'b\bar{b} + X \to \mu^+\mu^- b\bar{b} + X$, predominantly arising from $Z'bb$ coupling. However, we found it to be not promising even with 3000 fb^{-1} integrated luminosity, due primarily to three-body phase-space suppression. The same conclusion applies to $pp \to Z'b\bar{s} + X$, which gives direct access to the $Z'bs$ coupling.

The discovery potential of the Z' is rather limited due to the B_s-mixing constraint. The B_s-mixing constraint, however, is only indirect and is susceptible to the details of the UV completion of the effective model. In particular, we illustrated that the existence of a tiny but nonzero right-handed $Z'bs$ coupling g_{bs}^R accommodates a large LH $Z'bs$ coupling due to the cancellation in the B_s-mixing amplitude, without conflicting with the $b \to s\ell\ell$ global fits. In this case we found that discovery in both the $pp \to Z' + X$ and $pp \to Z'b + X$ processes may occur even with $\mathcal{O}(100)$ fb^{-1} integrated luminosity.

Comments on the subtlety of the implementation of the B_s-mixing constraint are in order (see also Sec. III). As mentioned above, a 30% enhancement in the B_s-mixing amplitude M_{12} by NP roughly corresponds to the 2σ upper limits by the latest global analyses of CKMfitter [83] and UTfit [84]. This may look rather tolerant, in view of the recent progress [86] in the estimation of the hadronic matrix element by lattice, which lead to $\sim 6\%$ uncertainty in M_{12}^{SM} [85]. This is because the central values of $|M_{12}/M_{12}^{SM}|$ are greater than unity in Refs. [83,84], while the Z' contribution always enhances $|M_{12}|$ relative to the SM value under the assumption of a real-valued g_{bs}^L with $g_{bs}^R = 0$. On the other hand, a recent study [77] finds the SM prediction of $\Delta m_{B_s^0} = 2|M_{12}|$ to be 1.8σ above the measured value, favoring $|M_{12}/M_{12}^{SM}|$ smaller than unity. This is opposite to the results by CKMfitter [83] and UTfit [84], although both UTfit (summer 2016 result) and Ref. [77] take into account the recent lattice result [86]. If the

result of Ref. [77] is the case, the Z' contribution may enhance $|M_{12}|$ only up to $\sim 1\%$ so that g_{bs}^L is strongly constrained. In this case the estimated signal significances at the LHC would shrink down to insignificant values for $|g_{bb}^L| \lesssim |g_{bs}^L|$, unless a tiny RH $Z'bs$ coupling exists for the cancellation in M_{12} and/or g_{bs}^L is close to pure imaginary so that it gives a negative contribution in M_{12}. The latter implies a nearly imaginary C_9^{NP} and would need a dedicated global analysis of $b \to s\ell\ell$ observables, as discussed in Ref. [77]. In any case, a consensus among the different groups seems to be still missing for the prediction of M_{12} in the SM, and a better understanding would be required for its calculation. At the same time, improvements in lattice calculations and determinations of CKM parameters will also facilitate a more precise SM prediction for M_{12}.

Although we considered $Z'bb$ and $Z'bs$ couplings to be the only couplings to the quark sector, the Z' may also couple to other quarks in general. For instance, if a nonzero $Z'cc$ coupling exists, the process $pp \to Z'c + X$ can be induced at the LHC. Such a process can mimic the $pp \to Z'b + X$ signature if the final state c-jet gets misidentified as a b-jet. This possibility cannot be excluded yet as pointed out in Ref. [118], where a procedure to disentangle $pp \to Z'c + X$ and $pp \to Z'b + X$ is discussed with the simultaneous application of both c and b tagging. We also remark that our estimation of the signal significances ignored various experimental uncertainties and the QCD corrections to the signal cross sections.

For illustration, we focused on $m_{Z'} = 200$ and 500 GeV. In general, heavier Z' are possible. However, due to the fall in the parton luminosity with the resonance mass, the achievable significances are lower than those of 200 and 500 GeV in both the $pp \to Z'$ and $pp \to Z'b$ processes.

Our results illustrate three possible scenarios for the LHC discovery and identification of a Z' that might be behind the $b \to s\ell\ell$ anomalies. The first one is the case with the minimal assumption, where the LH $Z'bs$ coupling is the only coupling to the quark sector. In this case, the discovery of the $pp \to Z' + X \to \mu^+\mu^- + X$ and $pp \to Z'b + X \to \mu^+\mu^- b + X$ processes may occur with the full HL-LHC data, but should be accompanied by a $\sim 30\%$ or larger enhancement in the B_s mixing, which can be tested following future improvements in the estimation of the B_s mixing. The second one is the case with a tiny but nonzero RH $Z'bs$ coupling such that the B_s mixing remains SM-like due to the cancellation of the Z' effects. In this case, the discovery of the two modes may occur with Run-3 data (or perhaps even Run-2 data); this scenario predicts a nonzero RH $b \to s$ current, with $C_9' \sim 0.1 C_9^{NP}$, which can be tested with improvements in $b \to s\ell\ell$ measurements by ATLAS, CMS, LHCb and Belle II. In particular, precise measurements of R_K and R_{K^*} by LHCb with Run-2 or a further data set may pin down the chiral structure of the $b \to s$ current. The third scenario is the case with a flavor-conserving $Z'bb$ coupling much larger than $Z'bs$. In this case, the two modes

may be discovered with Run-3 data without a significant effect in the B_s mixing and RH $b \to s$ current, but the role of the observed resonance in $b \to s\ell\ell$ is obscured.

Note added.—Recently, we noticed that the CMS 13 TeV 36 fb^{-1} result [119] for a heavy resonance search in the dilepton final state is now available. We find that the extracted upper limits [120] on g_{bb}^L from Ref. [119] are comparable to those from ATLAS [92] and do not change the conclusion of our results.

[1] R. Ammar *et al.* (CLEO Collaboration), Phys. Rev. Lett. **71,** 674 (1993).

[2] S. Descotes-Genon, J. Matias, M. Ramon, and J. Virto, J. High Energy Phys. 01 (2013) 048.

[3] R. Aaij *et al.* (LHCb Collaboration), Phys. Rev. Lett. **111,** 191801 (2013).

[4] R. Aaij *et al.* (LHCb Collaboration), J. High Energy Phys. 02 (2016) 104.

[5] R. Aaij *et al.* (LHCb Collaboration), Phys. Rev. Lett. **113,** 151601 (2014).

[6] R. Aaij *et al.* (LHCb Collaboration), J. High Energy Phys. 08 (2017) 055.

[7] R. Aaij *et al.* (LHCb Collaboration), J. High Energy Phys. 06 (2014) 133.

[8] R. Aaij *et al.* (LHCb Collaboration), J. High Energy Phys. 11 (2016) 047.

[9] R. Aaij *et al.* (LHCb Collaboration), J. High Energy Phys. 09 (2015) 179.

[10] R. Aaij *et al.* (LHCb Collaboration), J. High Energy Phys. 06 (2015) 115.

[11] ATLAS Collaboration, Report No. ATLAS-CONF-2017-023.

[12] A. M. Sirunyan *et al.* (CMS Collaboration), Phys. Lett. B **781,** 517 (2018).

[13] S. Wehle *et al.* (Belle Collaboration), Phys. Rev. Lett. **118,** 111801 (2017).

[14] T. Abe *et al.* (Belle-II Collaboration), arXiv:1011.0352.

[15] B. Capdevila, A. Crivellin, S. Descotes-Genon, J. Matias, and J. Virto, J. High Energy Phys. 01 (2018) 093.

[16] W. Altmannshofer, P. Stangl, and D. M. Straub, Phys. Rev. D **96,** 055008 (2017).

[17] G. D'Amico, M. Nardecchia, P. Panci, F. Sannino, A. Strumia, R. Torre, and A. Urbano, J. High Energy Phys. 09 (2017) 010.

[18] G. Hiller and I. Nisandzic, Phys. Rev. D **96,** 035003 (2017).

[19] L.-S. Geng, B. Grinstein, S. Jäger, J. Martin Camalich, X.-L. Ren, and R.-X. Shi, Phys. Rev. D **96,** 093006 (2017).

[20] M. Ciuchini, A. M. Coutinho, M. Fedele, E. Franco, A. Paul, L. Silvestrini, and M. Valli, Eur. Phys. J. C **77,** 688 (2017).

[21] A. Celis, J. Fuentes-Martin, A. Vicente, and J. Virto, Phys. Rev. D **96,** 035026 (2017).

[22] T. Hurth, F. Mahmoudi, D. Martinez Santos, and S. Neshatpour, Phys. Rev. D **96,** 095034 (2017).

[23] A. Karan, R. Mandal, A. K. Nayak, R. Sinha, and T. E. Browder, Phys. Rev. D **95,** 114006 (2017).

[24] W. Altmannshofer and D. M. Straub, Eur. Phys. J. C **73,** 2646 (2013).

[25] R. Gauld, F. Goertz, and U. Haisch, Phys. Rev. D **89,** 015005 (2014).

[26] A. J. Buras and J. Girrbach, J. High Energy Phys. 12 (2013) 009.

[27] R. Gauld, F. Goertz, and U. Haisch, J. High Energy Phys. 01 (2014) 069.

[28] A. J. Buras, F. De Fazio, and J. Girrbach, J. High Energy Phys. 02 (2014) 112.

[29] P. Ko, Y. Omura, and C. Yu, J. High Energy Phys. 01 (2014) 016.

[30] I. Ahmed, M. J. Aslam, and M. A. Paracha, Phys. Rev. D **89,** 015006 (2014).

[31] W. Altmannshofer, S. Gori, M. Pospelov, and I. Yavin, Phys. Rev. D **89,** 095033 (2014).

[32] B. Bhattacharya, A. Datta, D. London, and S. Shivashankara, Phys. Lett. B **742,** 370 (2015).

[33] A. Crivellin, G. D'Ambrosio, and J. Heeck, Phys. Rev. Lett. **114,** 151801 (2015).

[34] A. Crivellin, G. D'Ambrosio, and J. Heeck, Phys. Rev. D **91,** 075006 (2015).

[35] C. Niehoff, P. Stangl, and D. M. Straub, Phys. Lett. B **747,** 182 (2015).

[36] D. Aristizabal Sierra, F. Staub, and A. Vicente, Phys. Rev. D **92,** 015001 (2015).

[37] W. Altmannshofer and D. M. Straub, arXiv:1503.06199.

[38] A. Crivellin, L. Hofer, J. Matias, U. Nierste, S. Pokorski, and J. Rosiek, Phys. Rev. D **92,** 054013 (2015).

[39] A. Celis, J. Fuentes-Martin, M. Jung, and H. Serodio, Phys. Rev. D **92,** 015007 (2015).

[40] G. Bélanger, C. Delaunay, and S. Westhoff, Phys. Rev. D **92,** 055021 (2015).

[41] A. Falkowski, M. Nardecchia, and R. Ziegler, J. High Energy Phys. 11 (2015) 173.

[42] S. Descotes-Genon, L. Hofer, J. Matias, and J. Virto, J. High Energy Phys. 06 (2016) 092.

[43] B. Allanach, F. S. Queiroz, A. Strumia, and S. Sun, Phys. Rev. D **93,** 055045 (2016).

[44] A. J. Buras and F. De Fazio, J. High Energy Phys. 03 (2016) 010.

[45] K. Fuyuto, W.-S. Hou, and M. Kohda, Phys. Rev. D **93**, 054021 (2016).

[46] C.-W. Chiang, X.-G. He, and G. Valencia, Phys. Rev. D **93**, 074003 (2016).

[47] C. S. Kim, X.-B. Yuan, and Y.-J. Zheng, Phys. Rev. D **93**, 095009 (2016).

[48] W. Altmannshofer, M. Carena, and A. Crivellin, Phys. Rev. D **94**, 095026 (2016).

[49] J. Hisano, Y. Muramatsu, Y. Omura, and Y. Shigekami, J. High Energy Phys. 11 (2016) 018.

[50] W. Altmannshofer, C.-Y. Chen, P. S. Bhupal Dev, and A. Soni, Phys. Lett. B **762**, 389 (2016).

[51] P. Ko, T. Nomura, and H. Okada, Phys. Lett. B **772**, 547 (2017).

[52] D. Bhatia, S. Chakraborty, and A. Dighe, J. High Energy Phys. 03 (2017) 117.

[53] W.-S. Hou, M. Kohda, and T. Modak, Phys. Rev. D **96**, 015037 (2017).

[54] A. K. Alok, B. Bhattacharya, D. Kumar, J. Kumar, D. London, and S. U. Sankar, Phys. Rev. D **96**, 015034 (2017).

[55] S. Di Chiara, A. Fowlie, S. Fraser, C. Marzo, L. Marzola, M. Raidal, and C. Spethmann, Nucl. Phys. **B923**, 245 (2017).

[56] A. Greljo and D. Marzocca, Eur. Phys. J. C **77**, 548 (2017).

[57] A. K. Alok, B. Bhattacharya, A. Datta, D. Kumar, J. Kumar, and D. London, Phys. Rev. D **96**, 095009 (2017).

[58] C. Bonilla, T. Modak, R. Srivastava, and J. W. F. Valle, arXiv:1705.00915.

[59] J. Ellis, M. Fairbairn, and P. Tunney, Eur. Phys. J. C **78**, 238 (2018).

[60] F. Bishara, U. Haisch, and P. F. Monni, Phys. Rev. D **96**, 055002 (2017).

[61] R. Alonso, P. Cox, C. Han, and T. T. Yanagida, Phys. Lett. B **774**, 643 (2017).

[62] C.-W. Chiang, X.-G. He, J. Tandean, and X.-B. Yuan, Phys. Rev. D **96**, 115022 (2017).

[63] S. F. King, J. High Energy Phys. 08 (2017) 019.

[64] R. S. Chivukula, J. Isaacson, K. A. Mohan, D. Sengupta, and E. H. Simmons, Phys. Rev. D **96**, 075012 (2017).

[65] J. M. Cline and J. Martin Camalich, Phys. Rev. D **96**, 055036 (2017).

[66] P. Cox, C. Han, and T. T. Yanagida, J. High Energy Phys. 01 (2018) 037.

[67] S. Baek, Phys. Lett. B **781**, 376 (2018).

[68] M. C. Romao, S. F. King, and G. K. Leontaris, arXiv:1710.02349.

[69] P. Cox, C. Han, and T. T. Yanagida, J. Cosmol. Astropart. Phys. 01 (2018) 029.

[70] G. Faisel and J. Tandean, J. High Energy Phys. 02 (2018) 074.

[71] M. Dalchenko, B. Dutta, R. Eusebi, P. Huang, T. Kamon, and D. Rathjens, Phys. Rev. D **97**, 075035 (2018).

[72] B. C. Allanach, B. Gripaios, and T. You, J. High Energy Phys. 03 (2018) 021.

[73] D. Choudhury, A. Kundu, R. Mandal, and R. Sinha, arXiv:1712.01593.

[74] S. Antusch, C. Hohl, S. F. King, and V. Susic, arXiv:1712.05366.

[75] K. Fuyuto, H.-L. Li, and J.-H. Yu, arXiv:1712.06736.

[76] S. Raby and A. Trautner, Phys. Rev. D **97**, 095006 (2018).

[77] L. Di Luzio, M. Kirk, and A. Lenz, Phys. Rev. D **97**, 095035 (2018).

[78] M. Chala and M. Spannowsky, arXiv:1803.02364.

[79] A. J. Buras, S. Jäger, and J. Urban, Nucl. Phys. **B605**, 600 (2001).

[80] C. Patrignani et al. (Particle Data Group), Chin. Phys. C **40**, 100001 (2016) and 2017 update.

[81] B. Capdevila, S. Descotes-Genon, J. Matias, and J. Virto, J. High Energy Phys. 10 (2016) 075.

[82] A. Lenz, U. Nierste, J. Charles, S. Descotes-Genon, A. Jantsch, C. Kaufhold, H. Lacker, S. Monteil, V. Niess, and S. T'Jampens, Phys. Rev. D **83**, 036004 (2011).

[83] J. Charles et al., Phys. Rev. D **91**, 073007 (2015).

[84] M. Bona et al. (UTfit Collaboration), Phys. Rev. Lett. **97**, 151803 (2006); J. High Energy Phys. 03 (2008) 049; http://www.utfit.org, for updates.

[85] S. Aoki et al., Eur. Phys. J. C **77**, 112 (2017), http://flag.unibe.ch, for updates.

[86] A. Bazavov et al. (Fermilab, Lattice, and MILC Collaborations), Phys. Rev. D **93**, 113016 (2016).

[87] For a projection of the B_s-mixing constraint, see, e.g., the talk by M. Bona presented at ICHEP2016, Chicago, USA, August 2016, https://indico.cern.ch/event/432527/contributions/1071767/.

[88] A. J. Buras, J. Girrbach-Noe, C. Niehoff, and D. M. Straub, J. High Energy Phys. 02 (2015) 184.

[89] J. Brod, M. Gorbahn, and E. Stamou, Phys. Rev. D **83**, 034030 (2011).

[90] Y. Amhis et al., Eur. Phys. J. C **77**, 895 (2017) and online update at http://www.slac.stanford.edu/xorg/hflav.

[91] J. Grygier et al. (Belle Collaboration), Phys. Rev. D **96**, 091101 (2017).

[92] M. Aaboud et al. (ATLAS Collaboration), J. High Energy Phys. 10 (2017) 182. The $\sigma(pp \to Z' + X) \cdot \mathcal{B}(Z' \to \mu^+\mu^-)$ 95% C.L. upper limit is available, along with other auxiliaries, at https://atlas.web.cern.ch/Atlas/GROUPS/PHYSICS/PAPERS/EXOT-2016-05/.

[93] We digitize a figure for dimuon 95% C. L. upper limit obtained from https://atlas.web.cern.ch/Atlas/GROUPS/PHYSICS/PAPERS/EXOT-2016-05/ to extract the $\sigma(pp \to Z' + X) \cdot \mathcal{B}(Z' \to \mu^+\mu^-)$ upper limit for pole masses $m_{Z'} = 200$ and 500 GeV.

[94] J. Alwall, R. Frederix, S. Frixione, V. Hirschi, F. Maltoni, O. Mattelaer, H.-S. Shao, T. Stelzer, P. Torrielli, and M. Zaro, J. High Energy Phys. 07 (2014) 079.

[95] R. D. Ball, V. Bertone, S. Carrazza, L. Del Debbio, S. Forte, A. Guffanti, N. P. Hartland, and J. Rojo (NNPDF Collaboration), Nucl. Phys. **B877**, 290 (2013).

[96] W. Altmannshofer, S. Gori, M. Pospelov, and I. Yavin, Phys. Rev. Lett. **113**, 091801 (2014).

[97] S. R. Mishra et al. (CCFR Collaboration), Phys. Rev. Lett. **66**, 3117 (1991).

[98] U. Haisch and S. Westhoff, J. High Energy Phys. 08 (2011) 088.

[99] S. Schael et al. (ALEPH, DELPHI, L3, OPAL and SLD Collaborations, and LEP Electroweak Working Group, SLD Electroweak Group and SLD Heavy Flavour Group), Phys. Rep. **427**, 257 (2006).

[100] J. Fuster *et al.* (DELPHI Collaboration), Reports No. CERN-OPEN-99-393 and No. CERN-DELPHI-99-81.

[101] M. Pospelov, Phys. Rev. D **80**, 095002 (2009).

[102] F. Jegerlehner and A. Nyffeler, Phys. Rep. **477**, 1 (2009).

[103] R. Aaij *et al.* (LHCb Collaboration), Phys. Rev. Lett. **118**, 191801 (2017).

[104] A. Alloul, N. D. Christensen, C. Degrande, C. Duhr, and B. Fuks, Comput. Phys. Commun. **185**, 2250 (2014).

[105] T. Sjöstrand, S. Mrenna, and P. Skands, J. High Energy Phys. 05 (2006) 026.

[106] J. Alwall *et al.*, Eur. Phys. J. C **53**, 473 (2008).

[107] J. de Favereau, C. Delaere, P. Demin, A. Giammanco, V. Lemaître, A. Mertens, and M. Selvaggi (DELPHES 3 Collaboration), J. High Energy Phys. 02 (2014) 057.

[108] Y. Li and F. Petriello, Phys. Rev. D **86**, 094034 (2012).

[109] ATLAS-CMS recommended predictions for top-quark-pair cross sections, https://twiki.cern.ch/twiki/bin/view/LHCPhysics/TtbarNNLO.

[110] N. Kidonakis, Phys. Rev. D **82**, 054018 (2010).

[111] T. Gehrmann, M. Grazzini, S. Kallweit, P. Maierhöfer, A. von Manteuffel, S. Pozzorini, D. Rathlev, and L. Tancredi, Phys. Rev. Lett. **113**, 212001 (2014).

[112] M. Grazzini, S. Kallweit, D. Rathlev, and M. Wiesemann, Phys. Lett. B **761**, 179 (2016).

[113] F. Cascioli, T. Gehrmann, M. Grazzini, S. Kallweit, P. Maierhöfer, A. von Manteuffel, S. Pozzorini, D. Rathlev, L. Tancredi, and E. Weihs, Phys. Lett. B **735**, 311 (2014).

[114] G. Cowan, K. Cranmer, E. Gross, and O. Vitells, Eur. Phys. J. C **71**, 1554 (2011); **73**, 2501(E) (2013).

[115] R. Boughezal, X. Liu, and F. Petriello, Phys. Rev. D **94**, 074015 (2016).

[116] ATLAS Collaboration, Report No. ATLAS-CONF-2014-058.

[117] A. J. Buras, F. De Fazio, and J. Girrbach, J. High Energy Phys. 02 (2013) 116.

[118] W.-S. Hou, M. Kohda, and T. Modak, arXiv:1801.02579.

[119] A. M. Sirunyan *et al.* (CMS Collaboration), arXiv:1803.06292.

[120] The CMS analysis puts 95% C. L. upper limits on the quantity R_σ, which is defined as the ratio of dimuon production cross section via Z' to the one via Z or γ^* (in the dimuon-invariant mass range of 60–120 GeV): $R_\sigma = \frac{\sigma(pp \to Z'+X \to \mu^+\mu^-+X)}{\sigma(pp \to Z+X \to \mu^+\mu^-+X)}$. As in the case of the ATLAS limit, we digitize the figure for the dimuon final state to extract the limit on R_σ. If the Z' width is narrow, the R_σ can be interpreted as the limits on $\sigma(pp \to Z'+X) \cdot \mathcal{B}(Z' \to \mu^+\mu^-)$, with the multiplication of the SM prediction of $\sigma(pp \to Z+X)\mathcal{B}(Z \to \mu^+\mu^-) = 1928.0$ pb. See Ref. [53] for the details of how CMS limits are extracted.